



Article

Ag/Ag₂O as a Co-Catalyst in TiO₂ Photocatalysis: Effect of the Co-Catalyst/Photocatalyst Mass Ratio

Soukaina Akel ^{1,2,*}, Ralf Dillert ^{1,3} , Narmina O. Balayeva ¹, Redouan Boughaled ¹, Julian Koch ⁴, Mohammed El Azzouzi ² and Detlef W. Bahnemann ^{1,3,5,*} 

¹ Institut für Technische Chemie, Leibniz Universität Hannover, Callinstr. 3, D-30167 Hannover, Germany; dillert@iftc.uni-hannover.de (R.D.); balayeva@iftc.uni-hannover.de (N.O.B.); r.boughaled@gmail.com (R.B.)

² Laboratory of Spectroscopy, Molecular Modeling, Materials, Nanomaterials, Water and Environment, (LS3MN2E) Faculty of Sciences, University Mohammed V. BP 1014, Rabat 10000, Morocco; elazzouzim@hotmail.com

³ Laboratorium für Nano-und Quantenengineering, Leibniz Universität Hannover, Schneiderberg 39, D-30167 Hannover, Germany

⁴ Institut für Festkörperphysik, Leibniz Universität Hannover, Appelstraße 2, 30167 Hannover, Germany; koch@fkp.uni-hannover.de

⁵ Laboratory “Photoactive Nanocomposite Materials”, Saint-Petersburg State University, Ulyanovskaya Street 1, Peterhof, Saint-Petersburg 198504, Russia

* Correspondence: akel@iftc.uni-hannover.de (S.A.); bahnemann@iftc.uni-hannover.de or detlef.bahnemann@spbu.ru (D.W.B.); Tel.: +49-511-762-2773 (S.A.); +49-511-762-5560 (D.W.B.)

Received: 20 October 2018; Accepted: 4 December 2018; Published: 10 December 2018



Abstract: Mixtures and composites of Ag/Ag₂O and TiO₂ (P25) with varying mass ratios of Ag/Ag₂O were prepared, employing two methods. Mechanical mixtures (TM) were obtained by the sonication of a suspension containing TiO₂ and Ag/Ag₂O. Composites (TC) were prepared by a precipitation method employing TiO₂ and AgNO₃. Powder X-ray diffraction (XRD) and X-ray photoelectron spectroscopy (XPS) confirmed the presence of Ag(0) and Ag₂O. The activity of the materials was determined employing methylene blue (MB) as the probe compound. Bleaching of MB was observed in the presence of all materials. The bleaching rate was found to increase with increasing amounts of TiO₂ under UV/vis light. In contrast, the MB bleaching rate decreased with increasing TiO₂ content upon visible light illumination. XRD and XPS data indicate that Ag₂O acts as an electron acceptor in the light-induced reaction of MB and is transformed by reduction of Ag⁺, yielding Ag(0). As a second light-induced reaction, the evolution of molecular hydrogen from aqueous methanol was investigated. Significant H₂ evolution rates were only determined in the presence of materials containing more than 50 mass% of TiO₂. The experimental results suggest that Ag/Ag₂O is not stable under the experimental conditions. Therefore, to address Ag/Ag₂O as a (photo)catalytically active material does not seem appropriate.

Keywords: photocatalysis; silver(II) oxide; titanium dioxide; mechanical mixture; in situ deposition; hydrogen evolution

1. Introduction

Environmental problems related to water and air contamination, due to increasing world population and the resulting tremendous growth of industry and fuel combustion, have become a major concern of advanced science. In order to deal with this important problem, photocatalytic processes with employment of semiconductors are the most conventional approaches for water and air purification, along with alternative energy storage (e.g., H₂) [1–4].

To date, different semiconductor nanoparticles such as TiO_2 , ZnO , Fe_2O_3 , niobates, tantalates, and metal sulfides, and their underlying working mechanisms, have been investigated with the aim of increasing their photocatalytic activity. It is well known that, besides the ability to decontaminate polluted air and water, a photocatalyst should meet certain requirements such as cost efficiency, stability, non-toxicity, and broad range response towards incident light. TiO_2 is reported as the most durable photocatalyst, responding to all the above-mentioned requirements apart from broad range response to incident solar light due to its wide bandgap energy, (3.2 eV for anatase, 3.0 eV for rutile) which accounts for no more than 5% of the entire solar spectrum [1]. This lack of photocatalytic activity under visible light illumination allows the use of TiO_2 as a UV blocker in sunscreens [5]. The tremendous interest in modification of titanium dioxide with different metals and oxides, to enable absorption of lower energy states and increase stability, has been rising over the last 20 years. Nonetheless, the range of visible-light photocatalysts is still restricted. Thus, it is essential to discover new and efficient photocatalytic materials that are sensitive to visible light.

Ag_2O nanoparticles have been broadly utilized in various manufacturing areas as stabilizers, cleaning agents, electrode supplies, dyes, antioxidants, and catalysts for alkane activation and olefin [6,7]. Several papers have been published reporting the photocatalytic activity of Ag_2O , $\text{Ag}/\text{Ag}_2\text{O}$, $\text{Ag}_2\text{O}/\text{semiconductors}$, and $\text{Ag}/\text{Ag}_2\text{O}/\text{semiconductor}$ composites, and some reviews are available [8–33]. Ag_2O is reported to be a visible light active photocatalyst. However, due to its photosensitive and labile properties under incident light illumination, Ag_2O is infrequently employed alone as a main photocatalyst rather than as a co-catalyst [8].

Wang et al. investigated the photocatalytic performance of Ag_2O on the photocatalytic decolorization of methyl orange, rhodamine B, and phenol solution under fluorescent light irradiation, and concluded that the stability and high photocatalytic activity of Ag_2O is maintained by the partial formation of metallic Ag on its surface during the photodecomposition of organic compounds [9]. Jiang et al. also reported the decomposition of methyl orange under visible light, ultraviolet light, near-infrared (NIR) light, and sunlight irradiation, using silver oxide nanoparticle aggregation. The superb photo-oxidation performance of Ag_2O is kept almost constant after repeated exposure to light due to its narrow band gap, high surface area, and numerous crystal boundaries supplied by Ag_2O quantum dots [13]. Several authors have claimed that an $\text{Ag}/\text{Ag}_2\text{O}$ structure exhibits 'self-stability' [9,10] during a photocatalytic run, due to rapid electron transfer from the excited Ag_2O to $\text{Ag}(0)$ [12,20].

Visible light active nanocomposites of $\text{Ag}/\text{Ag}_2\text{O}/\text{TiO}_2$ have been synthesized using different methods, such as a microwave-assisted method [28], a low-temperature hydrothermal method [32], a one-step solution reduction process in the presence of potassium borohydride [22], a simple pH-mediated precipitation [23], and a sol-gel method [27]. Moreover, Su et al. developed a novel multilayer photocatalytic membrane, consisting of an $\text{Ag}_2\text{O}/\text{TiO}_2$ layer stacked on a chitosan sub-layer immobilized onto a polypropylene [31]. Light-induced hydrogen production via photoreforming of aqueous glycerol has been scrutinized, employing $\text{Ag}_2\text{O}/\text{TiO}_2$ catalysts prepared by a sol-gel method with varying content of Ag_2O (0.72–6.75 wt %) [30]. Hao et al. have reported that $\text{TiO}_2/\text{Ag}_2\text{O}$ nanowire arrays forming a p-n heterojunction are applicable for enhanced photo-electrochemical water splitting [33]. Hu et al. reported the photocatalytic degradation of tetracycline under UV, visible, NIR, and simulated solar light irradiation with the Z-scheme between visible/NIR light activated Ag_2O and UV light activated TiO_2 , using reduced graphene oxide as the electron mediator. They also investigated the stability of Ag_2O , $\text{Ag}_2\text{O}/\text{TiO}_2$, and $\text{Ag}_2\text{O}/\text{TiO}_2$ in combination with reduced graphene oxide as an electron mediator. A large amount of $\text{Ag}(0)$ was formed into Ag_2O and $\text{Ag}_2\text{O}/\text{TiO}_2$ after four cycles of tetracycline photodegradation under UV, visible, and NIR illumination [23]. Ren et al. also observed the light-induced reduction of Ag_2O during dye degradation in $\text{Ag}_2\text{O}/\text{TiO}_2$ suspensions. The authors suggested that the formation of $\text{Ag}(0)$ contributed to the high stability of their photocatalyst [29]. The stabilization of $\text{Ag}_2\text{O}/\text{TiO}_2$ photocatalysts by $\text{Ag}(0)$ formed at an initial stage of an experimental run has already been proposed earlier [11]. The photocatalytic stability of Ag-bridged Ag_2O nanowire

networks/TiO₂ nanotubes, which were fabricated by a simple electrochemical method, revealed only an insignificant loss in performance, with respect to photocatalytic degradation of the dye acid orange 7, under simulated solar light [15]. On the other hand, Kaur et al. reported a decrease of the degradation efficiency from 81% to 54%, after the third experimental run employing Ag₂O/TiO₂ as the photocatalyst and the drug levofloxacin as the probe compound [24]. Very recently, Mandari et al. synthesized plasmonic Ag₂O/TiO₂ photocatalysts, which could absorb visible light by the resonant oscillation of the conduction band electrons under visible light illumination. With this method, they were able to improve the efficiency of TiO₂ as a photocatalyst for hydrogen production by H₂O splitting under natural solar light. The authors observed the formation of Ag(0) by light-induced reduction of Ag₂O [26]. Light-induced reduction of Ag(I) to Ag(0) has also been reported for an Ag(0)/Ag(I) co-doped TiO₂ photocatalyst [34].

The preceding discussion of published experimental results provoked doubt on the stability of Ag₂O-containing photocatalysts under UV/vis illumination. Therefore, visible light harvesting Ag/Ag₂O//TiO₂ photocatalysts for water treatment and photocatalytic hydrogen generation were synthesized. To the best of our knowledge, physical Ag/Ag₂O//TiO₂ mixtures synthesized by the sonication of a suspension containing TiO₂ (P25) and a self-prepared Ag/Ag₂O were investigated for the first time. Ag/Ag₂O//TiO₂ composites, prepared in situ by a simple precipitation method employing TiO₂ and AgNO₃, were also prepared, in order to evaluate the effect of the synthesis method on the photocatalytic activity. Additionally, the effect of the mass ratio of Ag/Ag₂O was studied. The as-prepared mixtures and composites showed improved visible light activity for methylene blue (MB) bleaching, compared to blank TiO₂, and high photocatalytic H₂ production from a methanol-water mixture under artificial solar light illumination.

2. Results

2.1. Characterization of the Prepared Materials

The powder X-ray diffraction (XRD) patterns of Ag/Ag₂O, physical mixtures of Ag/Ag₂O//TiO₂ with increasing amounts of TiO₂ (20 mass% (TM 41), 50% (TM 11), and 80% (TM 14)), and in situ prepared Ag/Ag₂O//TiO₂ composites (20 mass% TiO₂ (TC 41), 50% (TC 11), and 80% (TC 14)) are shown in Figure 1. The XRD peaks for Ag/Ag₂O at 26.7°, 32.8°, 38.1°, 54.9°, 65.4°, and 68.8° perfectly correlate to the (110), (111), (200), (220), (311), and (222) crystal planes of cubic Ag₂O (JCPDS 41–1104). The three peaks at 44.3°, 64.7°, and 77.5° are indexed to the (200), (200), and (311) crystal planes of cubic Ag(0), respectively (JCPDS 04-0783) [35,36].

The TiO₂ containing mixtures (TM) and composites (TC) exhibit diffraction peaks at 25°, 38°, 48°, 54°, 55°, 63°, 69°, 71°, 75°, and 83°, which are attributed to the tetragonal phase of anatase TiO₂, whereas one peak at 27.8° corresponds to the tetragonal phase of rutile TiO₂. Figure 1a presents the patterns of the TM mixtures, where two phases of titania were present. The two strongest peaks of Ag₂O become more prominent, with the Ag₂O mass ratio increasing from TM 14 to TM 41. The small diffraction peaks situated at 44.4°, 64.2°, and 77.5° are indexed to the (200), (200), and (311) plane of metallic Ag(0) (JCPDS 04-0783) [20]. The strongest peak of Ag(111) might likely be masked by the TiO₂ peak at 2θ = 38°. The diffraction peaks in the TM mixture patterns correspond to the cubic structure of Ag₂O and the cubic structure of Ag [35,36]. Figure 1b illustrates the XRD patterns of the TC composites. As the figure shows, no significant difference between the two preparations methods was observed, except that in TiO₂-rich composites TC 11 and TC 14 no Ag₂O diffraction peaks were observed, suggesting a complete reduction of Ag₂O to metallic silver Ag(0) during the preparation of these composites. The XRD pattern of TiO₂ is presented for comparison. The diffractogram clearly indicates the presence of two TiO₂ phases with predominance of the anatase phase (JCPDS 21–1272).

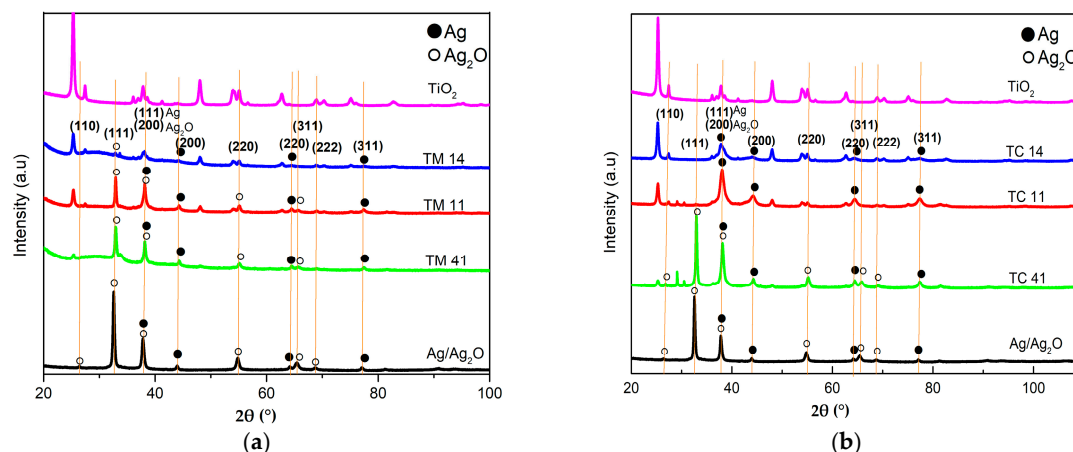


Figure 1. X-ray diffraction (XRD) patterns of (a) TiO₂ containing mixtures (TM), and (b) TiO₂ containing composites (TC). The diffractograms of Ag/Ag₂O and TiO₂ are included in both figures.

In order to investigate the oxidation states of the silver species present on the materials, X-ray photoelectron spectroscopy (XPS) was performed. The results of the XPS analysis for all samples are shown in Figure S3. The deconvolution of the high-resolution spectra for Ag 3d reveals that silver was present in more than one oxidation state in all samples. The binding energies of Ag 3d at 367.5 and 373.5 eV are assigned to the Ag 3d_{5/2} and Ag 3d_{3/2} photoelectrons respectively, indicating the presence of silver in the +1 oxidation state. The other two peaks of Ag 3d_{5/2} and Ag 3d_{3/2}, at 368.3 and 374.3 eV respectively, confirm the existence of silver in the Ag(0) state. These binding energies are in good agreement with the values reported for Ag(I) in Ag₂O and Ag(0) [16,37,38]. The peaks for O 1s, located in the ranges of 528.9–530.1 eV and 530.5–531.2 eV, are ascribed to O^{2−} in Ag₂O and TiO₂ respectively (Figure S3). From the Ti 2p core-level spectrum, two peaks at about 464.3 and 458.7 eV can be assigned to the Ti 2p_{1/2} and Ti 2p_{3/2} spin–orbital components respectively, which correspond to the characteristic peaks of Ti⁴⁺.

The SEM images of blank TiO₂, Ag/Ag₂O, TM mixtures, and TC composites are presented in Figure 2. Ag/Ag₂O showed well-defined particles with particle sizes ranging from 100 nm to 500 nm (Figure 2a). The small particles that contrast as white spots correspond to the metallic silver Ag(0) distributed on the surface of silver oxide, which is in agreement with the XRD results. The EDX reveals that the sample contained Ag and O without any other impurities (Figure S1).

Figure 2b–d shows SEM images of the physical mixtures of Ag/Ag₂O with TiO₂. It becomes obvious from these images that Ag/Ag₂O changed its shape during preparation of the mixtures by sonification of aqueous suspensions of the oxides. The increasing loading of the Ag₂O platelets with TiO₂ is also clearly recognizable in these figures. In the Ag/Ag₂O//TiO₂ mixture with the highest mass fraction of TiO₂ (TM 14), the appearance was apparently determined by the titanium dioxide distributed over the underlying surface of the Ag₂O platelets (Figure 2d). This was also reflected in the specific surface area (SSA) of the materials. The TiO₂ (P25) used in this work is known to have an average diameter and specific surface area of 21 nm and about 50 m² g^{−1}, respectively [39]. The specific surface area of the Ag/Ag₂O synthesized in this work was determined to be 2.7 m² g^{−1}. As expected, the specific surface area of the Ag/Ag₂O//TiO₂ mixtures was found to increase with increasing TiO₂ content (Table 1), resulting in a SSA of 38.5 m² g^{−1} for TM 14.

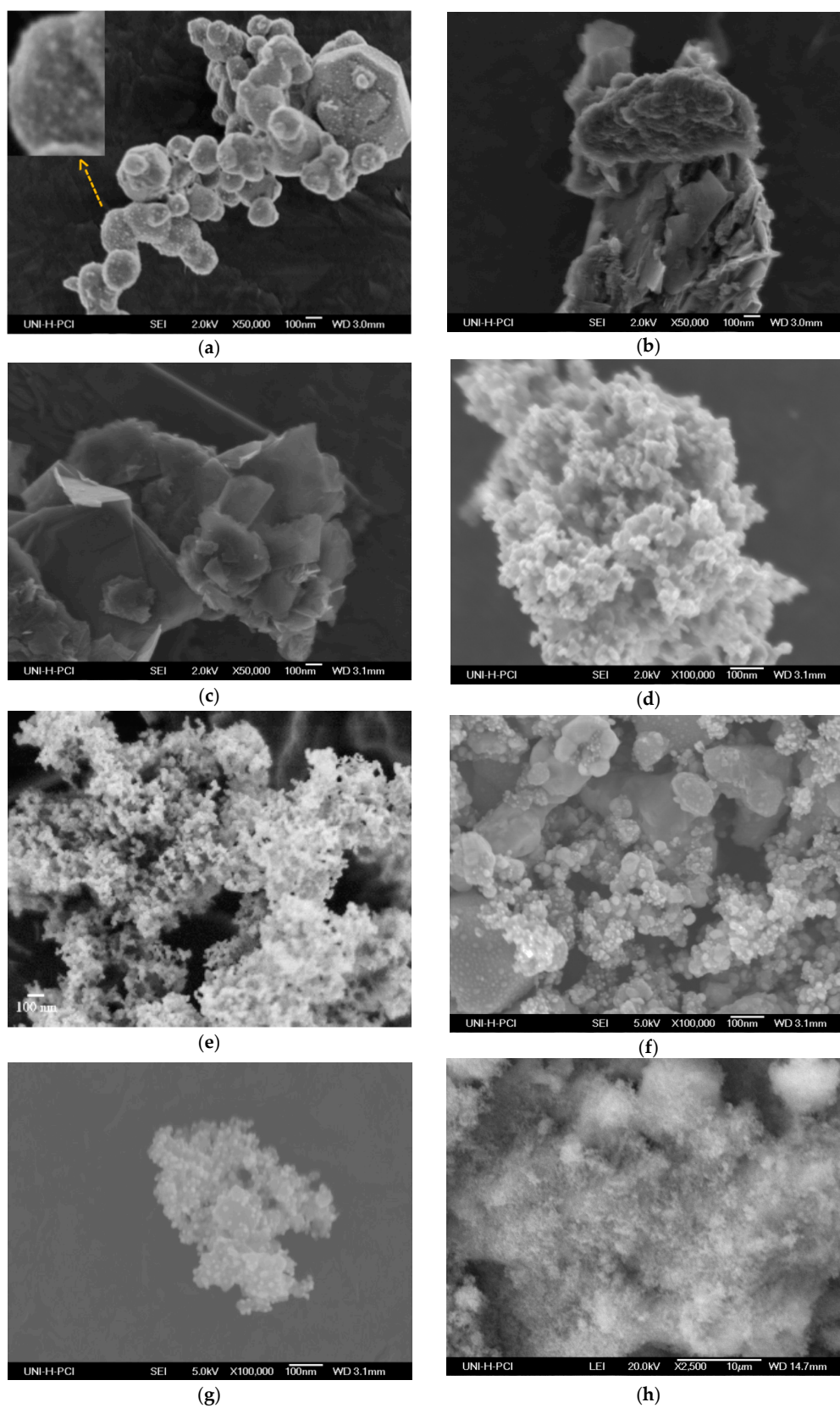


Figure 2. SEM pictures of (a) Ag/Ag₂O, (b) TM 41, (c) TM 11, (d) TM 14, (e) TiO₂ (P25), (f) TC 41, (g) TC 11, and (h) TC 14.

SEM images of the TC composites are presented in Figure 2f–h. The image of the TiO₂-poor composite TC 41 clearly shows the large Ag/Ag₂O particles covered with TiO₂ (Figure 2f). The specific surface area of this composite was determined to be 8.4 m² g^{−1}, thus being equal within the limits of the experimental error to the surface area of the corresponding physical mixture TC 41 (SSA = 9.7 m² g^{−1}). The images of the composites richer in TiO₂ (TC 11 and TC 14) seemed to be dominated by aggregates or agglomerates of small TiO₂ particles.

The optical properties of TiO₂ and the as-prepared Ag-containing mixtures and composites were investigated by UV/vis diffuse reflectance spectroscopy (Figure 3). Ag/Ag₂O, as well as the TM, and TC materials, had a dark brown to black color. They displayed strong absorption over the whole UV and visible range (200 nm–800 nm). TiO₂ showed only the absorption band below 405 nm, which matches the band gap energy of 3.06 eV calculated from the formula $\lambda = 1239.8/E_{bg}$ due to the charge transfer from O (valence band) to Ti (conduction band).

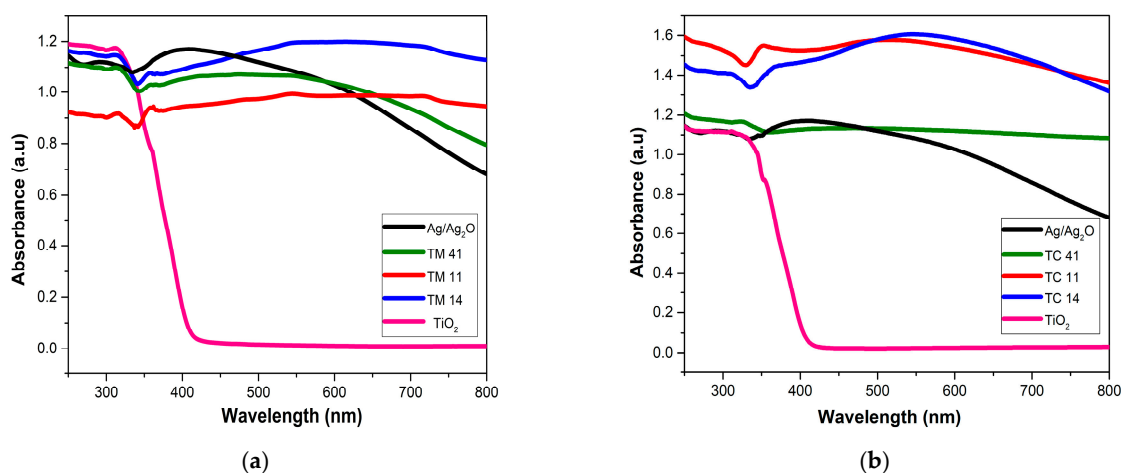


Figure 3. UV/vis diffuse reflectance spectra of (a) TiO₂, Ag/Ag₂O, TM mixtures, and (b) TC composites.

Ag/Ag₂O exhibited a band gap energy < 1.5 eV, which is in agreement with the reported value of 1.3 ± 0.3 eV [40]. The scattering of the reported values might be due to different particle diameters, as shown for TiO₂ [41]. Electrochemical measurements in suspensions yielded flat band potentials of −0.4 V and +0.3 V vs. NHE for TiO₂ and Ag₂O, respectively. The value measured here for the flat band potential of Ag₂O is also in reasonably good agreement with published values [42,43].

2.2. Photocatalytic Performance of the Materials

The photocatalytic activity of all materials described above was investigated, employing methylene blue (MB) as the probe compound. The materials in aqueous suspensions were excited by the full output of a xenon lamp (UV/vis illumination), and by Xe light after passing a UV cut-off filter (≥410 nm, vis illumination). Figure 4 illustrates the bleaching of an aqueous solution of MB and the MB-containing suspensions. Photolysis of MB (initiated by the direct excitation of the probe compound) was observed under both UV/vis and visible light illumination. The bleaching of MB was significantly accelerated by the presence of Ag/Ag₂O. Under UV/vis illumination, Ag/Ag₂O was found to be nearly as active as TiO₂ (P25), which is well known to be a very efficient photocatalyst suitable to degrade MB [44] (Figure 4a). In the presence of Ag/Ag₂O, MB was bleached very rapidly even when exposed to visible light. As expected, TiO₂, having a bandgap energy of 3.1 eV, was found to be inactive under vis illumination (Figure 4c).

In the presence of mixtures of Ag/Ag₂O with TiO₂, MB was bleached under UV/vis illumination only in the presence of the TiO₂-rich TM 14, with a significantly increased rate compared to the rate of MB photolysis. In suspensions containing TM 41 and TM 11, the rate of bleaching was almost the same

as the rate of photolysis (Figure 4a). Exposure to visible light in the presence of the Ag/Ag₂O-rich TM 41 resulted in bleaching of MB with a slightly increased rate. In contrast, the TiO₂-rich mixtures TM 11 and TM 14 were virtually inactive under this illumination condition (Figure 4c).

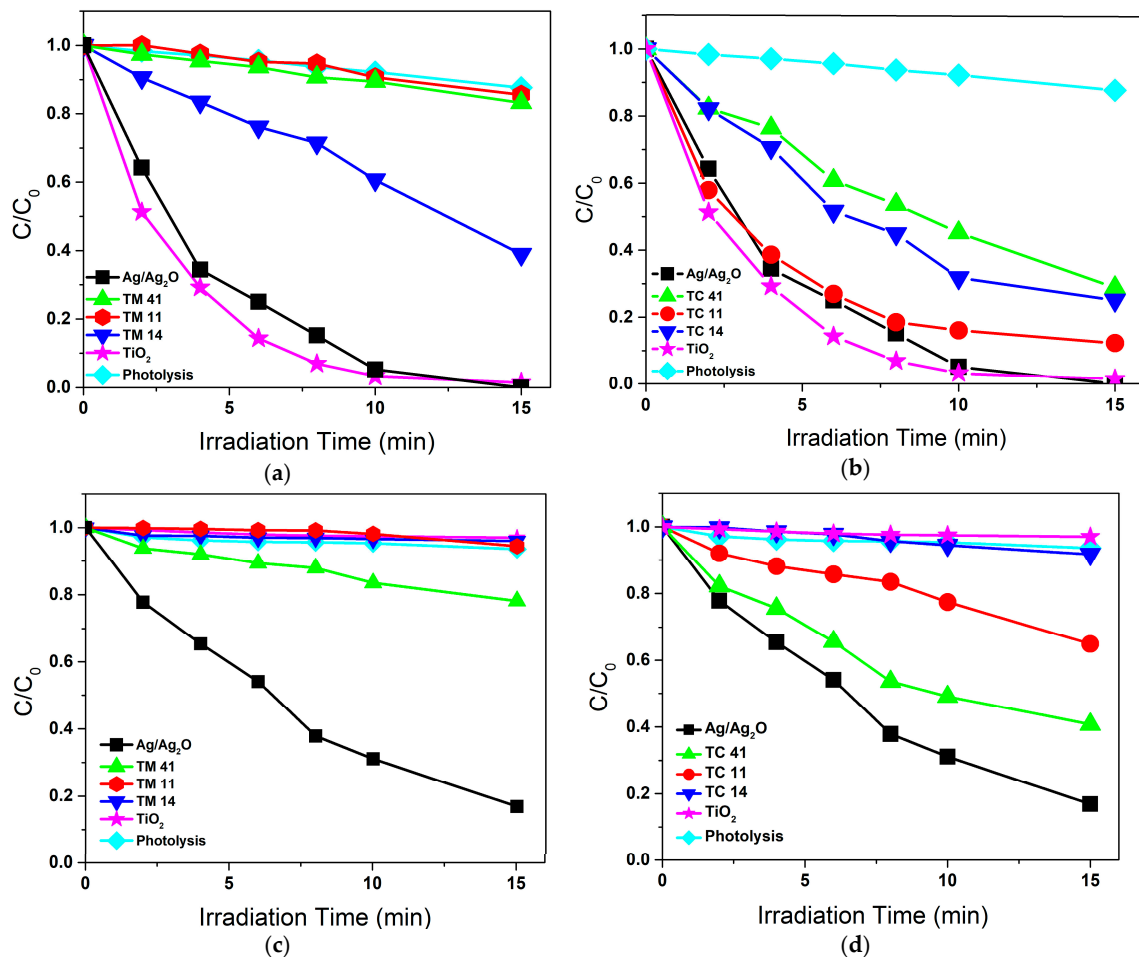


Figure 4. Bleaching of MB in the presence of Ag/Ag₂O, TiO₂, the TM mixtures and the TC composites under UV/vis (a,b) and under vis light only (c,d).

In the presence of the composites TC, MB was bleached with significantly faster reaction rates than the rate of photolysis when exposed to UV/vis and visible light. The rates were, however, lower than the rate of bleaching in the presence of the bare TiO₂ (Figure 4b,d). Interestingly, while increasing the amount of TiO₂ in the TC composites, the visible light activity of the materials seemed to decrease, thus confirming the essential influence of Ag/Ag₂O on MB bleaching under illumination with wavelengths ≥ 410 nm.

As a second test reaction for the activity of the materials, the UV/vis light-induced evolution of molecular hydrogen by reforming of aqueous methanol was used. Figure 5 shows the amount of H₂ vs. illumination time in the presence of TiO₂, Ag/Ag₂O, and the prepared mixtures and composites. No H₂ evolution was observed in the presence of Ag/Ag₂O and the Ag/Ag₂O-rich TM 41. In the presence of all other materials, the evolution of H₂ was detected. However, large amounts of H₂ were only evolved with the materials TM 14 (104 μ mol/6 h) and TC 11 (174 μ mol/6 h).

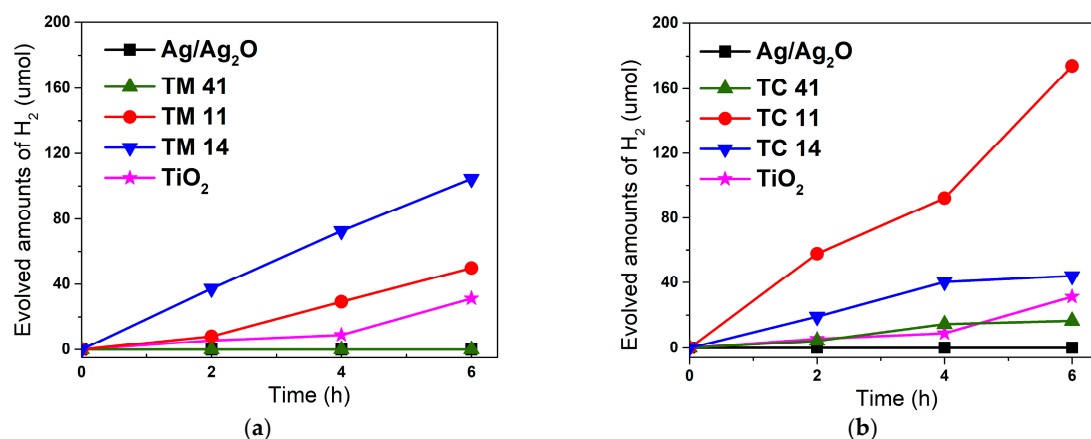


Figure 5. The amount of H_2 evolved from aqueous methanol under UV/vis illumination of Ag/Ag₂O, TiO₂, (a) TM mixtures and (b) TC composites vs. illumination time.

Many authors have reported that the kinetic behavior of photocatalytic reactions can be described by a Langmuir–Hinshelwood rate law, with the two limiting cases of zero-order and first-order kinetics [45,46]. To calculate the initial rates r_0 of the bleaching of methylene blue, first-order kinetics have been assumed ($r_0 = kC_0$). To determine the rate constant k , the data given in Figure 4 have therefore been fitted with $C = C_0 \exp(-kt)$. The initial rates are given in Table 1.

Table 1. Brunauer-Emmet-Teller (BET) surface area, initial rates of methylene blue (MB) bleaching and H_2 generation in the presence of Ag/Ag₂O, TiO₂, the TM mixtures and the TC composites.

Sample	Preparation Method	Composition	SSA	r_0 (MB)	r_0 (MB)	r (H_2)
			$m^2 g^{-1}$	UV/vis $mg L^{-1} min^{-1}$	vis $mg L^{-1} min^{-1}$	UV/vis $\mu mol h^{-1}$
Photolysis	-	-	-	0.08	0.05	-
Ag/Ag ₂ O	in situ	Ag/Ag ₂ O	2.7	2.64	1.17	-
TM 41	mechanical mixture	Ag/Ag ₂ O//TiO ₂ (20% TiO ₂)	9.7	0.12	0.17	-
TM 11	mechanical mixture	Ag/Ag ₂ O//TiO ₂ (50% TiO ₂)	22.6	0.09	0.03	9
TM 14	mechanical mixture	Ag/Ag ₂ O//TiO ₂ (80% TiO ₂)	38.5	0.55	0.03	17
TiO ₂	-	TiO ₂	50	3.08	0.03	5
TC 41	in situ	Ag/Ag ₂ O//TiO ₂ (20% TiO ₂)	8.4	0.81	0.61	3
TC 11	in situ	Ag/Ag ₂ O//TiO ₂ (50% TiO ₂)	20.1	2.03	0.27	28
TC 14	in situ	Ag/Ag ₂ O//TiO ₂ (80% TiO ₂)	22.1	1.00	0.05	8

3. Discussion

3.1. The Photocatalytic Activity of Ag/Ag₂O

It is well known that methylene blue is photocatalytically oxidized in the presence of TiO₂ under illumination with photons having an energy equal to or larger than the bandgap energy of the semiconductor. The photocatalytic degradation of methylene blue in the presence of molecular oxygen is reported to follow Equation (1) [44].



The energetic positions of the valence and conduction bands of TiO₂ and Ag₂O, and the reduction potentials of some species (possibly) present in the surrounding electrolyte are shown in Figure 6. As becomes obvious from this Figure, the conduction band electrons generated by UV illumination of TiO₂ are able to reduce O₂ adsorbed at the semiconductor surface. From a thermodynamic point of view, valence band holes at the TiO₂ surface have an energy suitable to oxidize H₂O/OH[−], yielding OH radicals. These OH radicals are generally assumed to be the oxidizing species in photocatalytic MB degradation.

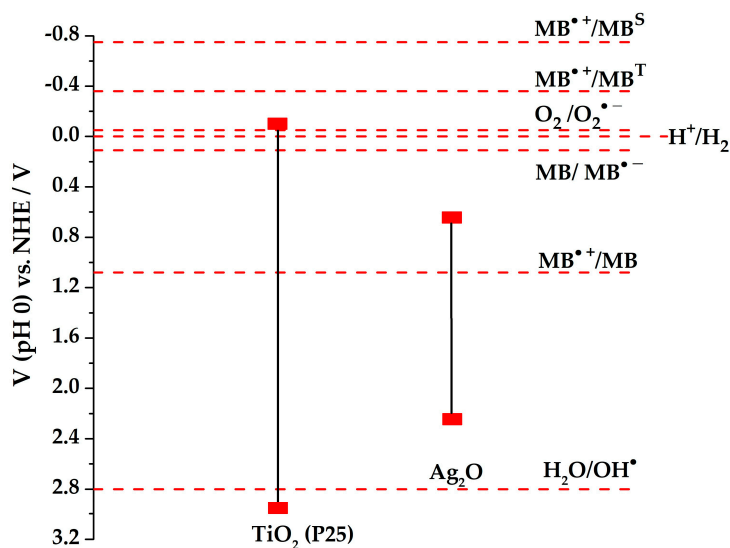
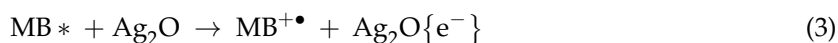
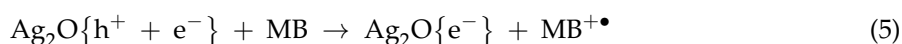


Figure 6. The electrochemical potentials (vs. NHE) of the valence and conduction bands of TiO_2 and Ag_2O , and the reduction potentials of some species (possibly) present in the surrounding electrolyte. MB, $\text{MB}^{\bullet-}$, $\text{MB}^{\bullet+}$, MB^{T} , and MB^{S} denote the MB ground state, the semi-reduced MB, the oxidized MB, the excited triplet state, and the excited singlet state of MB, respectively. The one electron reduction potentials have been calculated with data given in References [44,47,48].

With the assumption that the flat band potential of Ag_2O , which has been determined to be +0.3 V vs. NHE at pH 7, was equal to the conduction band edge of this semiconductor, and a bandgap energy $E_g = 1.5$ eV, the valence band position was calculated to be +2.0 V vs. NHE. Xu and Schoonen reported a value of +0.2 V vs. NHE for the energy of the Ag_2O conduction band [49]. As becomes obvious from Figure 6, excited Ag_2O was neither able to reduce O_2 nor to oxidize $\text{H}_2\text{O}/\text{OH}^-$. Consequently, the mechanism of MB bleaching observed in the presence of $\text{Ag}/\text{Ag}_2\text{O}$ (Figure 4 and Table 1) was different from the MB degradation mechanism in the presence of TiO_2 . A possible explanation for the decolorization of MB in the presence of $\text{Ag}/\text{Ag}_2\text{O}$ is that MB is excited by light of suitable wavelength (Equation (2), $\text{MB}^* = \text{MB}^{\text{S}}$ and or MB^{T}), which is subsequently followed by electron injection into the conduction band of Ag_2O (Equation (3)).



As an alternative to these reactions, the direct oxidation of MB by valence band holes according to



has to be considered. Both mechanisms require an electron transfer between Ag_2O and MB. Despite the low surface area available for this reaction, the electron transfer between the solid and the probe compound appears to be very efficient.

It is well known that Ag_2O is sensitive to light and decomposes under illumination. However, it has been suggested that $\text{Ag}(0)$ being present in $\text{Ag}/\text{Ag}_2\text{O}$ acts as an electron sink and accepts the conduction band electron of Ag_2O , thus inhibiting the reduction of Ag^+ and stabilizing the Ag_2O [9,10,12,20]. However, the possibility cannot be excluded that Ag^+ is reduced during the processes given in the Equations (2)–(5), yielding $\text{Ag}(0)$, since no other suitable electron acceptor is available. Regardless of whether the electrons reduce Ag^+ or become stored in $\text{Ag}(0)$, $\text{Ag}/\text{Ag}_2\text{O}$ is not acting as a photocatalyst, because the material changes irreversibly during the reaction.

The potential of the Ag_2O conduction band electron is more positive than the reduction potential of the H^+/H_2 couple (Figure 6). Consequently, light-induced proton reduction yielding H_2 is thermodynamically impossible in suspensions containing only $\text{Ag}/\text{Ag}_2\text{O}$. This is in accordance with the experimental results reported in Section 2.2.

3.2. The Photocatalytic Activity of Physical $\text{Ag}/\text{Ag}_2\text{O}/\text{TiO}_2$ Mixtures

3.2.1. Bleaching of Methylene Blue

When irradiated with light at wavelengths ≥ 410 nm, methylene blue was found to be bleached in the presence of $\text{Ag}/\text{Ag}_2\text{O}$, and mixtures of this material with TiO_2 . The rate of MB bleaching decreased with increasing amounts of TiO_2 . Of course, TiO_2 itself was found to be photocatalytically inactive, since it was not excited under this illumination condition (Figure 4c and Table 1). The electron transfer reaction resulting in the observed bleaching of the MB solution occurred at the surface of the Ag_2O , as discussed in Section 3.1. According to the SEM images (Figure 2a–d), the surface of the Ag_2O was increasingly covered by TiO_2 as the content of this oxide in the mixture increased. The interfacial electron transfer was inhibited by this TiO_2 layer (Figure 7). The reaction rates suggest that this inhibition increased with increasing amounts of TiO_2 on the $\text{Ag}/\text{Ag}_2\text{O}$ surface. Consequently, the TiO_2 -rich mixtures TM 11 and TM 14 exhibited rates of bleaching almost the same as the rate of photolysis in homogeneous solution (Table 1). Interfacial electron transfer from excited MB to TiO_2 (which is thermodynamically possible; cf. Figure 6) obviously did not contribute significantly, since no MB bleaching was observed under visible light illumination of suspensions containing only this photocatalyst.



Figure 7. Possible mechanism of MB bleaching by Ag_2O and Ag_2O -containing mixtures and composites under visible light illumination.

The situation was different when the TM mixtures were illuminated with UV/vis light. The rate of MB bleaching in the presence of the $\text{Ag}/\text{Ag}_2\text{O}/\text{TiO}_2$ mixtures was found to increase with increasing TiO_2 content. However, the rates were always lower than the rates determined for suspensions containing only $\text{Ag}/\text{Ag}_2\text{O}$ or bare TiO_2 (Figure 4a and Table 1). These rates cannot be explained solely by the optical properties of the suspensions. Of course, as the $\text{Ag}/\text{Ag}_2\text{O}$ content increases, more UV photons are absorbed by Ag_2O . They are thus no longer available for the excitation of the TiO_2 that results in decreasing amounts of charge carriers in the TiO_2 and, consequently, decreasing rates of MB degradation. However, the MB bleaching rate calculated for the TiO_2 -rich TM 14 mixture suggests that not all photogenerated charge carriers were used in the desired MB bleaching reaction, but some were lost by reactions between excited TiO_2 and $\text{Ag}/\text{Ag}_2\text{O}$, resulting in the reduction of Ag^+ .

XRD measurements revealed the reduction of Ag^+ during the light-induced bleaching of MB under UV/vis illumination. The ratios of the peak intensities corresponding to Ag_2O and TiO_2 of the mixture TM 41 and the composite TC 41 were significantly lower after two experimental runs than before illumination (Figure 8). On the other hand, the ratios of the peak intensities attributed to metallic Ag and TiO_2 obviously increased. In the case of the $\text{Ag}/\text{Ag}_2\text{O}/\text{TiO}_2$ mixture TM 11, apart from the TiO_2 peaks, the only visible XRD peaks could be assigned to AgCl and $\text{Ag}(0)$ after illumination of a suspension containing MB (Figure S2). The new peaks in the diffractogram, which are indexed to AgCl , were possibly formed by a reaction between Ag^+ and Cl^- known to be present

at the surface of TiO_2 P25 [39]. This reaction certainly explains the decrease of the Ag_2O peaks in the diffractogram. However, this explanation does not exclude that Ag_2O is also transformed by a light-induced reduction reaction, yielding $\text{Ag}(0)$.

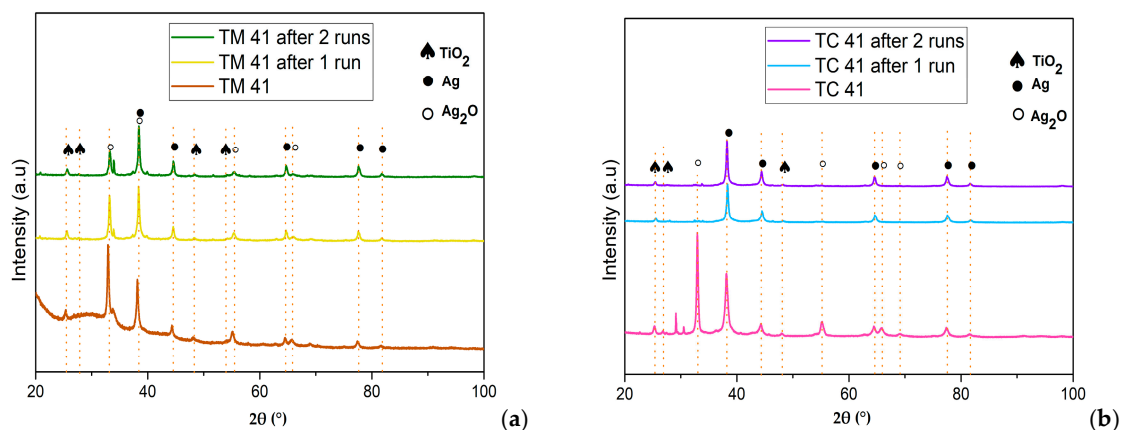


Figure 8. XRD patterns of (a) TM 41 and (b) TC 41 after two cycles of MB bleaching employing UV/vis light.

The conclusion from the XRD data, that Ag(I) was reduced yielding Ag(0) during the light-induced bleaching of MB in the presence of the mixture TM 41, is supported by the results of the analysis of XPS data taken before and after two experimental runs (Figure 9a,b and Figure S3). It becomes obvious from Figure 9a that the $\text{Ag } 3d_{5/2}$ and $\text{Ag } 3d_{3/2}$ peaks of Ag_2O in the mixture TM 41 decreased in intensity and broadened, while the $\text{Ag(0) } 3d_{5/2}$ and $\text{Ag(0) } 3d_{3/2}$ peaks increased in intensity after two photocatalytic reactions. Furthermore, the deconvolution of the $\text{O } 1s$ peaks denotes that the peak corresponding to the Ag-O bond had a lower intensity compared to the same peak observed before the reaction, indicating significant changes occurred during the light-induced MB bleaching reaction (Figure 9b). These changes were mainly due to the light-induced reduction of Ag^+ yielding Ag(0) . Again, the condition of stability of a catalyst was not satisfied.

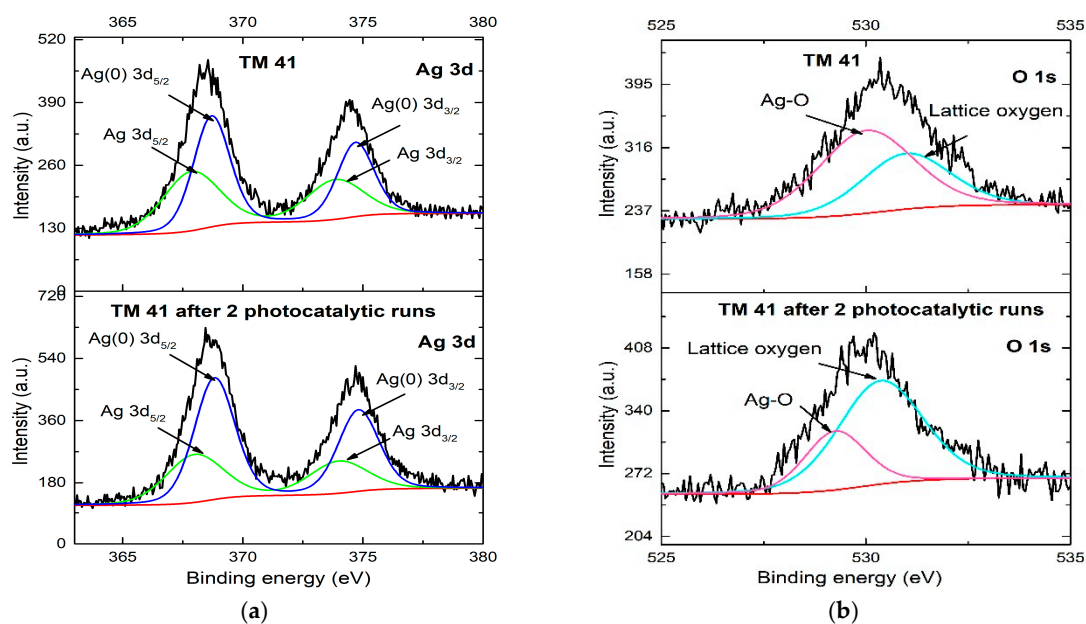


Figure 9. Cont.

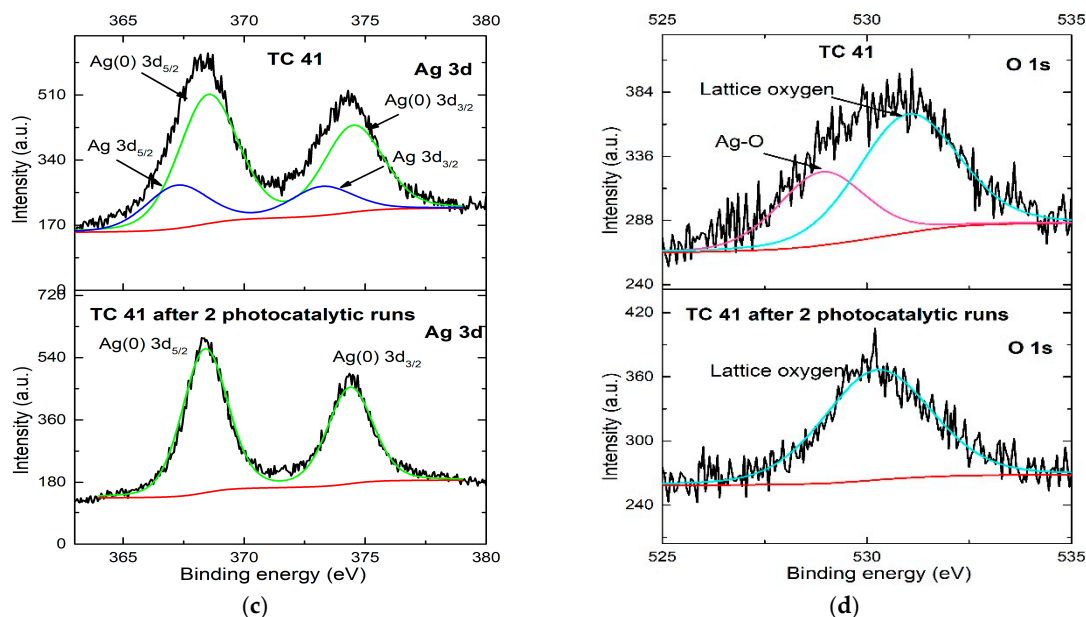


Figure 9. High-resolution XPS spectra of the Ag 3d and O 1s signals of TM 41 (a,b) and TC 41 (c,d) before and after two experimental runs.

3.2.2. Light-Induced Hydrogen Evolution

From a thermodynamic point of view, excited TiO_2 is able to transfer a conduction band electron to a proton present at the photocatalyst surface (Figure 6). This electron transfer is, however, known to be a kinetically inhibited process. Therefore, it is necessary to deposit an electrocatalyst at the TiO_2 surface, which accelerates the interfacial electron transfer. $\text{Ag}(0)$ is known to be a suitable, though relatively inactive, electrocatalyst [50,51]. In this work as well, pure TiO_2 showed only a very low photocatalytic activity with regard to H_2 evolution from aqueous methanol. When using the TM materials, a significant increase in the amount of H_2 evolved (consequently corresponding with an increase in the reaction rate) during six hours of illumination of the mixture was observed with increasing TiO_2 content (Figure 5a and Table 1). On the one hand, this can be explained by the fact that a significant portion of the UV photons was absorbed by Ag_2O being inactive under this illumination condition, and thus was not available for the desired H_2 evolution reaction. However, this portion decreased with increasing TiO_2 amount of the mixture. On the other hand, some of the TiO_2 conduction band electrons were transferred to the Ag_2O , where they were consumed to reduce Ag^+ to $\text{Ag}(0)$. These electrons were therefore also not available for the desired reaction. Obviously, these undesired electron losses are lower the higher the mass fraction of TiO_2 in the physical mixture, resulting in increasing H_2 evolution rates with increasing mass fraction of TiO_2 .

3.3. The Photocatalytic Activity of $\text{Ag}/\text{Ag}_2\text{O}/\text{TiO}_2$ Composites

3.3.1. Bleaching of Methylene Blue

When irradiated with light at wavelengths ≥ 410 nm, methylene blue was found to be bleached in the presence of the three TC composites (Figure 4d and Table 1). All TC composites exhibited a higher activity than the corresponding TM mixtures. As in the case of the TM materials, the rate of MB bleaching decreased with increasing amounts of TiO_2 . The increased reaction rates for MB bleaching in the presence of Ag_2O containing solids, compared to the rate of photolysis under visible light illumination, were explained in Section 3.2.1 with an interfacial electron transfer from (excited) MB to Ag_2O (cf. Figure 7). However, the experimental result is surprising when it is considered that the surfaces of the composites were smaller than the surfaces of the corresponding TM mixtures. A possible explanation may be due to the preparation method. For the TC materials, the $\text{Ag}/\text{Ag}_2\text{O}$

was prepared in a TiO_2 suspension. Therefore, the $\text{Ag}/\text{Ag}_2\text{O}$ was attached on the surface of the TiO_2 particles. In contrast, in the TM mixtures large $\text{Ag}/\text{Ag}_2\text{O}$ particles were covered by TiO_2 , hindering the electron transfer from excited MB to the Ag_2O , as discussed in Section 3.2.2.

The rate of MB bleaching in the presence of TC composite was significantly higher under UV/vis than under visible light illumination. As observed for the TM materials, the bleaching rates were lower in suspensions containing the composites than in suspensions containing only $\text{Ag}/\text{Ag}_2\text{O}$ or TiO_2 (Figure 4b and Table 1).

XRD and XPS data indicate that Ag(I) was reduced, yielding Ag(0) , during the light-induced bleaching reaction of MB in the presence of the composite TC 41. A stabilization of Ag_2O by metallic silver, as claimed by several authors [9–12,20,29], was not observed. No XRD peaks that can be attributed Ag_2O , were observed after two experimental runs of the composite. However, the ratios of the peak intensities due to metallic Ag and TiO_2 obviously increased (Figure 8b). No Ag $3d_{5/2}$ and Ag $3d_{3/2}$ peaks, which can be attributed to Ag(I) , were present either in the deconvoluted XPS spectra obtained after two experimental runs (Figure 9c and Figure S3). The XPS peak, which was attributed to the presence of Ag-O, also disappeared during the light-induced reaction (Figure 9d and Figure S3).

These observations support the statement made above that $\text{Ag}/\text{Ag}_2\text{O}$ cannot be called a photocatalyst. The XRD pattern shown in Figure 8b as well as the XPS data presented in the Figure 9c,d clearly evince that the $\text{Ag}:\text{Ag}_2\text{O}$ ratio changed during the light-induced bleaching of MB. Thus, the condition for a catalyst to exit a chemical reaction unchanged is not satisfied.

3.3.2. Light-Induced Hydrogen Evolution

The three TC composites were found to be able to promote light-induced H_2 evolution from aqueous methanol. The calculated reaction rates were significantly larger than those of the corresponding TM mixtures. The highest H_2 evolution rate was observed in the presence of TC 11 (Figure 5b and Table 1), which was also characterized by a high MB bleaching rate under UV/vis illumination. A possible mechanistic explanation for the high activity of the TC 11 composite is based on the assumption of synergistic effects, due to the presence of both Ag(0) and Ag_2O at the TiO_2 surface (Figure 10). TiO_2 is excited by UV photons. The photogenerated conduction band electrons migrated to the Ag(0) attached to the TiO_2 surface. In a subsequent step, interfacial electron transfer from Ag(0) to protons present in the surrounding electrolyte occurred, thus yielding molecular hydrogen. The valence band hole inside the TiO_2 particle was filled by an electron from an attached Ag_2O particle. Methanol was oxidized by this hole in the valence band of the Ag_2O . According to this mechanism, Ag(0) acts as an electron sink, thus decreasing the electron-hole recombination, and as electrocatalyst for the hydrogen evolution reaction, while Ag_2O is an electrocatalyst for the oxidation reaction of methanol yielding methanal. The supposition made here, that the methanol oxidation occurs at the Ag_2O surface via electron transfer to the valence band of the excited TiO_2 , has already been proclaimed earlier [16,19,23,26]. It should be emphasized again that the energy of an electron in the conduction band of the Ag_2O employed in this study is insufficient to reduce a proton (Figure 6). Consequently, excitation of TiO_2 is a prerequisite for photocatalytic reforming of methanol. TiO_2 is known to be a relatively inactive material for the photocatalytic reduction of protons. High evolution rates of molecular hydrogen are observed only in the presence of a co-catalyst. Ag_2O was found here to be an unsuitable co-catalyst for the hydrogen evolution reaction, since electron transfer from the excited TiO_2 can only occur into the conduction band of this material. The photocatalytic activities of the composites and mixtures discussed here are thus determined to a considerable extent by the competition between interfacial electron transfer to protons in the surrounding electrolyte, and to silver ions in Ag_2O . The mechanism of the photocatalytic hydrogen evolution by reforming of organic compounds in the presence of the mixtures and composites employed in this study does not contradict the mechanism discussed for $\text{Ag}/\text{Ag}_2\text{O}/\text{TiO}_2$ samples, which contain Ag_2O with a significantly more negative conduction band energy than TiO_2 [17,24,26,33].

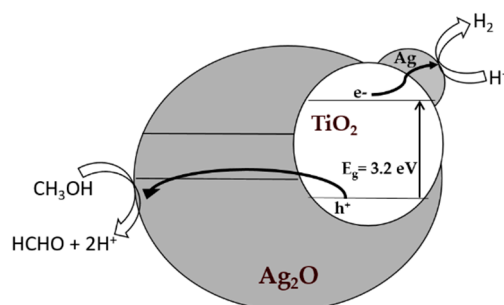


Figure 10. Mechanism of hydrogen evolution from aqueous methanol under UV/vis illumination.

Changes in the respective mass fractions of TiO_2 , Ag, and Ag_2O at constant total mass of the solid in suspension may have several impacts on the rate of hydrogen evolution. Increasing mass fractions of UV absorbing and scattering Ag and Ag_2O reduces the number of photons to be absorbed by the TiO_2 , thus reducing the H_2 evolution rate. A reduction of the mass fraction of metallic Ag may possibly slow down the interfacial electron transfer to the proton, while a reduction of the mass fraction of Ag_2O might negatively affect the oxidation reaction. It should also be noted that Ag_2O can act as a sink for a TiO_2 conduction band electron (cf. Figure 6). These partially opposing effects may be responsible for the observed differences in the H_2 evolution rates in the presence of the various TC composites (and TM mixtures).

4. Experimental Section

4.1. Materials

Titania P25 (TiO_2) with a mixture of anatase (80%) and rutile (20%) crystal phase, and a specific surface area of $50.1 \text{ m}^2 \text{ g}^{-1}$, was kindly provided by Evonik, Essen, Germany. Silver nitrate (99%, Sigma Aldrich Chemie GmbH, München, Germany), sodium hydroxide pellets (99%, Carl Roth, Karlsruhe, Germany), methanol (99.9%, Carl Roth), and methylene blue (Sigma Aldrich) were used without further purification. Deionized water with a resistivity of $18.2 \text{ M}\Omega \cdot \text{cm}$ was obtained from a Sartorius Arium 611 device (Sartorius Göttingen, Germany) and used for the preparation of all aqueous solutions and suspensions.

4.2. Synthetic Methods

4.2.1. Preparation of Ag/ Ag_2O

An amount of AgNO_3 was dissolved in 50 mL of distilled water. The obtained solution was stirred for 30 min. Subsequently, 50 mL NaOH (0.2 M) was added dropwise. The resulting suspension was stirred for another 30 min to promote hydrolysis, and centrifuged, washed with distilled water three times, and dried at 70°C for 24 h.

4.2.2. Preparation of TM Mixtures

The samples were obtained by mixing the self-prepared Ag_2O with TiO_2 at mass ratios of 4:1 (20 mass% TiO_2), 1:1 (50 mass% TiO_2), and 1:4 (20 mass% TiO_2) with water. The suspensions were sonicated for 1.5 h and dried at 70°C for 24 h. The Ag/ Ag_2O // TiO_2 with 20%, 50%, and 80% of TiO_2 were nominated as TM 41, TM 11, and TM 14, respectively. For purpose of comparison, a TiO_2 sample was prepared by the same procedure without the addition of Ag/ Ag_2O .

4.2.3. Preparation of TC Composites

The TC composites were prepared by a published precipitation method [25,29]. A measured amount of TiO_2 was suspended in 50 mL of distilled water, and the calculated amount of AgNO_3

corresponding to the desired mass ratio of Ag_2O was added to the solution. The obtained suspension was stirred for 30 min. A volume of 50 mL 0.2 M NaOH was added dropwise. The resulting suspension was stirred for another 30 min to promote hydrolysis and centrifuged, washed with distilled water three times and dried at 70 °C for 24 h. The Ag/ Ag_2O // TiO_2 with 20 mass%, 50 mass%, and 80 mass% of TiO_2 were denoted as TC 41, TC 11, and TC 14, respectively.

4.3. Characterization of the Materials

The crystalline structure of the catalysts was measured by powder X-ray diffraction XRD (D8 Advance system, Bruker, Billerica, MA, USA), using a Cu $K\alpha$ radiation source with a wavelength of $\lambda = 0.154178 \text{ \AA}$ over a 2θ range from 20° to 100°, with a 0.011° step width. The morphology of the prepared materials was determined using a scanning electron microscope (SEM), employing a JEOL JSM-6700F field emission instrument (Tokyo, Japan) with a resolution of 100 nm and 1 μm using an EDXS detector. Measurements of X-ray photoelectron spectra were carried out using a Leybold Heraeus (Cologne, Germany) with X-ray source, Mg & Al anode, nonmonochromatic, hemispherical analyzer, 100 mm radius. Data analysis was performed using XPSPEAK 4.1 software (Hong Kong, China). The energy of the C1s-line was set to 284.8 eV and used as reference for the data correction. Diffuse reflectance UV–Vis spectroscopy was employed using a spectrophotometer (Varian Spectrophotometer Cary-100 Bio, Agilent technologies, Santa Clara, CA, USA) at room temperature. Barium sulfate was used as a standard for 100% reflection. The specific surface area (SSA) of the samples was calculated by N_2 adsorption–desorption measurements, employing the Brunauer-Emmet-Teller (BET) method using a FlowSorb II 2300 apparatus from Micromeritics Instrument Company (Corp., Norcross, GA, USA). Prior to these measurements, the samples were evacuated at 180 °C for 1 h. Measurements of photocurrents and flat band potentials were performed with an electrochemical analyzer using three electrodes employing an Iviumstat potentiostat (Ivium Technologies bv, Eindhoven, The Netherlands). Films of the samples were used as the working electrode, after being coated on cleaned fluorine doped tin oxide (FTO) coated glass using the doctor blade method and calcinated at 400 °C for 2 h. These working electrodes were prepared by grinding 100 mg of the photocatalysts and 50 mg polyethylene glycol with one drop of Triton, followed by addition of 200 μL of deionized water and a sufficient amount of ethanol. An Ag/AgCl electrode (3 M NaCl, +209 mV vs. NHE) and a platinum coil were used as the reference electrode and the counter electrode, respectively. Potassium nitrate aqueous solution (0.1 M) was used as the electrolyte. The impedance spectra were recorded in the range between the chosen potential from -1 V to $+1 \text{ V}$ at frequencies of 10, 100, and 1000 Hz with 20 mV amplitude vs. Ag/AgCl. The capacitance was plotted against V , and the flat band was calculated from the intercept of the plot. (i.e., a plot of C^{-2} vs. V , where C was the capacitance and V was the potential across the space charge layer).

4.4. Photocatalytic Measurements

4.4.1. Methylene Blue Degradation

The apparatus used for carrying out of the photocatalytic degradation reactions consisted of a double jacket cylindrical reactor with a 230 mL volume, which circulated with cold water to maintain the ambient reaction. A volume of 200 mL of aqueous solution of methylene blue (MB, 10 mg L^{-1}) and 200 mg of photocatalysts were used for each reaction experiment. A 300 W Xenon arc lamp (Müller Elektronik-Optik, Moosinning, Germany) was used both as the UV/vis light source and as the vis light source by placing a UV cut-off filter ($\geq 410 \text{ nm}$) in the light path. The lamp was started 30 min before the degradation experiments to ensure maximum emission. Aliquots (1.5 mL) of the suspensions were collected at given time intervals (0, 2, 4, 6, 8, 10, 15, and 30 min), centrifuged to remove the solid, and analyzed immediately with the UV–Vis spectrophotometer.

4.4.2. Photocatalytic Hydrogen Formation

The photocatalytic H₂ generation experiments were conducted in quartz vials (capacity of 10 mL) under illumination with a 1000 W Xenon lamp (Hönle UV Technology, Gräfelfing, Germany; Sol 1200 solar). An amount of 6 mg of the photocatalyst was suspended in 6 mL aqueous methanol (10 vol% methanol). The suspension was purged with argon for 20 min to remove the air, and the quartz vial was sealed with a specially made rubber septum degassed for sampling. The amount of H₂ gas evolved during the photocatalytic reaction was quantified every two hours using a gas chromatograph (Shimadzu GC-8A, Shimadzu Deutschland GmbH, Duisburg, Germany) equipped with thermal conductivity detector (TCD) and 60/80 molecular sieve 5 Å column.

5. Conclusions

Ag/Ag₂O was found to enhance the rate of light-induced bleaching of aqueous methylene blue under both UV/vis and vis illumination, in comparison to the bleaching in homogeneous solution. Even in suspensions containing mixtures and composites of Ag/Ag₂O with TiO₂ (P25), with varying mass ratios of Ag/Ag₂O (20%, 50%, and 80%), the reaction rate was slightly increased under these illumination conditions. However, the bleaching rate of methylene blue was lower in the presence of the composites and mixtures than the rate measured for bare Ag/Ag₂O. It is therefore suggested that the bleaching of methylene blue is initiated by an interfacial electron transfer from the excited organic probe compound to Ag₂O. TiO₂ layers covering the Ag₂O seem to inhibit this electron transfer. Since Ag₂O can transfer an electron neither to dissolved molecular oxygen nor to a proton for thermodynamic reasons, it is assumed that Ag⁺ is reduced to Ag(0) in the processes investigated here. Results of XRD and XPS measurements support this assumption, and indicate that Ag/Ag₂O is not stable under the experimental conditions employed in this study. A stabilization of Ag₂O by metallic silver, as occasionally claimed, was not observed. Therefore, to address Ag/Ag₂O as a (photo)catalytically active material does not seem appropriate.

Supplementary Materials: The following are available online at <http://www.mdpi.com/2073-4344/8/12/647/s1>, Figure S1. EDX diagrams of all prepared photocatalysts. Figure S2. XRD patterns of TM 11 photocatalyst after one cycle of MB bleaching employing UV/vis light. Figure S3. XPS spectra of Ag 3d, O 1s and Ti 2p in the Ag/Ag₂O, TM and TC materials. Figure S4. Emission spectrum of the used Xenon lamp. Figure S5. UV/vis spectra of aqueous methylene blue solutions obtained during illumination with visible light in the presence of Ag/Ag₂O. Figure S6. Calibration curve for H₂ experiment.

Author Contributions: Experiments and analysis: S.A.; XPS measurements: J.K.; Redaction of manuscript: S.A., R.D. & R.B.; Review: R.D.; R.B. & N.O.B.; Scientific support: R.D.; Supervision: D.W.B. & M.E.A.

Funding: This research received no external funding.

Acknowledgments: The authors wish to thank Luis Granone for XRD measurements and Stephanie Melchers for SEM/EDAX images.

Conflicts of Interest: The authors declare no conflict of interest.

References

1. Bahnemann, D.W. Mechanisms of Organic Transformations on Semiconductor Particles. In *Photochemical Conversion and Storage of Solar Energy; Proceedings of the Eighth International Conference on Photochemical Conversion and Storage of Solar Energy, IPS-8, Palermo, Italy, 15–20 July 1990*; Pelizzetti, E., Schiavello, M., Eds.; Springer Science/Kluwer Academic Publishers: Dordrecht, The Netherlands; Boston, MA, USA, 1991; pp. 251–276.
2. Hoffmann, M.R.; Martin, S.T.; Choi, W.; Bahnemann, D.W. Environmental Applications of Semiconductor Photocatalysis. *Chem. Rev.* **1995**, *95*, 69–96. [[CrossRef](#)]
3. Bahnemann, D.W. Photocatalytic Detoxification of Polluted Waters. In *Environmental Photochemistry*; Boule, P., Ed.; Springer: Berlin/Heidelberg, Germany, 1999; pp. 285–351.
4. Fujishima, A.; Rao, T.N.; Tryk, D.A. Titanium Dioxide Photocatalysis. *J. Photochem. Photobiol. C Photochem. Rev.* **2000**, *1*, 1–21. [[CrossRef](#)]

5. Reinoso, J.J.; Álvarez-Docio, C.M.; Ramírez, V.Z.; Fernández, J.F. Hierarchical Nano ZnO-Micro TiO₂ Composites: High UV Protection Yield Lowering Photodegradation in Sunscreens. *Ceram. Int.* **2018**, *44*, 2827–2834. [[CrossRef](#)]
6. Wang, X.; Wu, H.-F.; Kuang, Q.; Huang, R.-B.; Xie, Z.-X.; Zheng, L.-S. Shape-Dependent Antibacterial Activities of Ag₂O Polyhedral Particles. *Langmuir* **2010**, *26*, 2774–2778. [[CrossRef](#)]
7. Zou, J.; Xu, Y.; Hou, B.; Wu, D.; Sun, Y. Self-Assembly Ag₂O Nanoparticles into Nanowires with the Aid of Amino-Functionalized Silica Nanoparticles. *Powder Technol.* **2008**, *183*, 122–126. [[CrossRef](#)]
8. Lalitha, K.; Reddy, J.K.; Phanikrishna Sharma, M.V.; Kumari, V.D.; Subrahmanyam, M. Continuous Hydrogen Production Activity over Finely Dispersed Ag₂O/TiO₂ Catalysts from Methanol:Water Mixtures under Solar Irradiation: A Structure-Activity Correlation. *Int. J. Hydrogen Energy* **2010**, *35*, 3991–4001. [[CrossRef](#)]
9. Wang, X.; Li, S.; Yu, H.; Yu, J.; Liu, S. Ag₂O as a New Visible-Light Photocatalyst: Self-Stability and High Photocatalytic Activity. *Chem. A Eur. J.* **2011**, *17*, 7777–7780. [[CrossRef](#)]
10. Wang, G.; Ma, X.; Huang, B.; Cheng, H.; Wang, Z.; Zhan, J.; Qin, X.; Zhang, X.; Dai, Y. Controlled Synthesis of Ag₂O Microcrystals with Facet-Dependent Photocatalytic Activities. *J. Mater. Chem.* **2012**, *22*, 21189. [[CrossRef](#)]
11. Chen, F.; Liu, Z.; Liu, Y.; Fang, P.; Dai, Y. Enhanced Adsorption and Photocatalytic Degradation of High-Concentration Methylene Blue on Ag₂O-modified TiO₂-based Nanosheet. *Chem. Eng. J.* **2013**, *221*, 283–291. [[CrossRef](#)]
12. Hu, X.; Hu, C.; Wang, R. Enhanced Solar Photodegradation of Toxic Pollutants by Long-Lived Electrons in Ag–Ag₂O Nanocomposites. *Appl. Catal. B Environ.* **2015**, *176–177*, 637–645. [[CrossRef](#)]
13. Jiang, W.; Wang, X.; Wu, Z.; Yue, X.; Yuan, S.; Lu, H.; Liang, B. Silver Oxide as Superb and Stable Photocatalyst under Visible and Near-Infrared Light Irradiation and Its Photocatalytic Mechanism. *Ind. Eng. Chem. Res.* **2015**, *54*, 832–841. [[CrossRef](#)]
14. Li, J.; Fang, W.; Yu, C.; Zhou, W.; Zhu, L.; Xie, Y. Ag-Based Semiconductor Photocatalysts in Environmental Purification. *Appl. Surf. Sci.* **2015**, *358*, 46–56. [[CrossRef](#)]
15. Liu, C.; Cao, C.; Luo, X.; Luo, S. Ag-bridged Ag₂O Nanowire Network/TiO₂ Nanotube Array p–n Heterojunction as a Highly Efficient and Stable Visible Light Photocatalyst. *J. Hazard. Mater.* **2015**, *285*, 319–324. [[CrossRef](#)]
16. Ren, H.-T.; Jia, S.-Y.; Zou, J.-J.; Wu, S.-H.; Han, X. A facile Preparation of Ag₂O/P25 Photocatalyst for Selective Reduction of Nitrate. *Appl. Catal. B Environ.* **2015**, *176–177*, 53–61. [[CrossRef](#)]
17. Kumar, D.P.; Reddy, N.L.; Karthik, M.; Neppolian, B.; Madhavan, J.; Shankar, M.V. Solar Light Sensitized p-Ag₂O/n-TiO₂ Nanotubes Heterojunction Photocatalysts for Enhanced Hydrogen Production in Aqueous-Glycerol Solution. *Sol. Energy Mater. Sol. Cells* **2016**, *154*, 78–87. [[CrossRef](#)]
18. Kumar, R.; El-Shishtawy, R.M.; Barakat, M.A. Synthesis and Characterization of Ag-Ag₂O/TiO₂@polypyrrole Heterojunction for Enhanced Photocatalytic Degradation of Methylene Blue. *Catalysts* **2016**, *6*, 76. [[CrossRef](#)]
19. Wei, N.; Cui, H.; Song, Q.; Zhang, L.; Song, X.; Wang, K.; Zhang, Y.; Li, J.; Wen, J.; Tian, J. Ag₂O Nanoparticle/TiO₂ Nanobelt Heterostructures with Remarkable Photo-Response and Photocatalytic Properties under UV, Visible and Near-Infrared Irradiation. *Appl. Catal. B Environ.* **2016**, *198*, 83–90. [[CrossRef](#)]
20. Yang, H.; Tian, J.; Li, T.; Cui, H. Synthesis of Novel Ag/Ag₂O Heterostructures with Solar Full Spectrum (UV, Visible and Near-Infrared) Light-Driven Photocatalytic Activity and Enhanced Photoelectrochemical Performance. *Catal. Commun.* **2016**, *87*, 82–85. [[CrossRef](#)]
21. Zhang, J.; Liu, H.; Ma, Z. Flower-Like Ag₂O/Bi₂MoO₆ p-n Heterojunction with Enhanced Photocatalytic Activity under Visible Light Irradiation. *J. Molec. Catal. A Chem.* **2016**, *424*, 37–44. [[CrossRef](#)]
22. Cui, Y.; Ma, Q.; Deng, X.; Meng, Q.; Cheng, X.; Xie, M.; Li, X.; Cheng, Q.; Liu, H. Fabrication of Ag-Ag₂O/reduced TiO₂ Nanophotocatalyst and its Enhanced Visible Light Driven Photocatalytic Performance for Degradation of Diclofenac Solution. *Appl. Catal. B Environ.* **2017**, *206*, 136–145. [[CrossRef](#)]
23. Hu, X.; Liu, X.; Tian, J.; Li, Y.; Cui, H. Towards Full-Spectrum (UV, Visible, and Near-Infrared) Photocatalysis: Achieving an All-Solid-State Z-Scheme between Ag₂O and TiO₂ Using Reduced Graphene Oxide as the Electron Mediator. *Catal. Sci. Technol.* **2017**, *7*, 4193–4205. [[CrossRef](#)]
24. Kaur, A.; Salunke, D.B.; Umar, A.; Mehta, S.K.; Sinha, A.S.K.; Kansal, S.K. Visible Light Driven Photocatalytic Degradation of Fluoroquinolone Levofloxacin Drug Using Ag₂O/TiO₂ Quantum Dots: A Mechanistic Study and Degradation Pathway. *New J. Chem.* **2017**, *41*, 12079–12090. [[CrossRef](#)]

25. Liu, B.; Mu, L.; Han, B.; Zhang, J.; Shi, H. Fabrication of $\text{TiO}_2/\text{Ag}_2\text{O}$ Heterostructure with Enhanced Photocatalytic and Antibacterial Activities under Visible Light Irradiation. *Appl. Surf. Sci.* **2017**, *396*, 1596–1603. [CrossRef]
26. Mandari, K.K.; Kwak, B.S.; Police, A.K.R.; Kang, M. In-Situ Photo-Reduction of Silver Particles and their SPR Effect in Enhancing the Photocatalytic Water Splitting of $\text{Ag}_2\text{O}/\text{TiO}_2$ Photocatalysts under Solar Light Irradiation: A Case Study. *Mater. Res. Bull.* **2017**, *95*, 515–524. [CrossRef]
27. Olya, M.E.; Vafaei, M.; Jahangiri, M. Modeling of Acid Dye Decolorization by $\text{TiO}_2\text{-Ag}_2\text{O}$ Nano-Photocatalytic Process Using Response Surface Methodology. *J. Saudi Chem. Soc.* **2017**, *21*, 633–642. [CrossRef]
28. Prakoso, S.P.; Taufik, A.; Saleh, R. $\text{Ag}/\text{Ag}_2\text{O}/\text{TiO}_2$ Nanocomposites: Microwave-Assisted Synthesis, Characterization, and Photosonocatalytic Activities. *IOP Conf. Ser. Mater. Sci. Eng.* **2017**, *188*, 012029. [CrossRef]
29. Ren, H.-T.; Yang, Q. Fabrication of $\text{Ag}_2\text{O}/\text{TiO}_2$ with Enhanced Photocatalytic Performances for Dye Pollutants Degradation by a pH-Induced Method. *Appl. Surf. Sci.* **2017**, *396*, 530–538. [CrossRef]
30. Wang, C.; Cai, X.; Chen, Y.; Cheng, Z.; Luo, X.; Mo, S.; Jia, L.; Shu, R.; Lin, P.; Yang, Z.; et al. Efficient Hydrogen Production from Glycerol Photoreforming Over $\text{Ag}_2\text{O-TiO}_2$ Synthesized by a Sol-Gel Method. *Int. J. Hydrogen Energy* **2017**, *42*, 17063–17074. [CrossRef]
31. Zhao, Y.; Tao, C.; Xiao, G.; Su, H. Controlled Synthesis and Wastewater Treatment of $\text{Ag}_2\text{O}/\text{TiO}_2$ Modified Chitosan-Based Photocatalytic Film. *RSC Adv.* **2017**, *7*, 11211–11221. [CrossRef]
32. Deng, A.; Zhu, Y. Synthesis of $\text{TiO}_2/\text{SiO}_2/\text{Ag}/\text{Ag}_2\text{O}$ and $\text{TiO}_2/\text{Ag}/\text{Ag}_2\text{O}$ Nanocomposite Spheres with Photocatalytic Performance. *Res. Chem. Intermed.* **2018**, *44*, 4227–4243. [CrossRef]
33. Hao, C.; Wang, W.; Zhang, R.; Zou, B.; Shi, H. Enhanced Photoelectrochemical Water Splitting with $\text{TiO}_2@\text{Ag}_2\text{O}$ Nanowire Arrays via p-n Heterojunction Formation. *Sol. Energy Mater. Sol. Cells* **2018**, *174*, 132–139. [CrossRef]
34. Liu, R.; Wang, P.; Wang, X.; Yu, H.; Yu, J. UV- and Visible-Light Photocatalytic Activity of Simultaneously Deposited and Doped $\text{Ag}/\text{Ag(I)-TiO}_2$ Photocatalyst. *J. Phys. Chem. C* **2012**, *116*, 17721–17728. [CrossRef]
35. Kang, J.-G.; Sohn, Y. Interfacial Nature of Ag Nanoparticles Supported on TiO_2 Photocatalysts. *J. Mater. Sci.* **2012**, *47*, 824–832. [CrossRef]
36. Jiang, B.; Hou, Z.; Tian, C.; Zhou, W.; Zhang, X.; Wu, A.; Tian, G.; Pan, K.; Ren, Z.; Fu, H. A Facile and Green Synthesis Route Towards Two-Dimensional $\text{TiO}_2@\text{Ag}$ Heterojunction Structure with Enhanced Visible Light Photocatalytic Activity. *CrystEngComm* **2013**, *15*, 5821. [CrossRef]
37. Hammond, J.S.; Gaarenstroom, S.W.; Winograd, N. X-ray Photoelectron Spectroscopic Studies of Cadmium- and Silver-Oxygen Surfaces. *Anal. Chem.* **1975**, *47*, 2193–2199. [CrossRef]
38. Zaccheo, B.A.; Crooks, R.M. Stabilization of Alkaline Phosphatase with $\text{Au}@ \text{Ag}_2\text{O}$ Nanoparticles. *Langmuir* **2011**, *27*, 11591–11596. [CrossRef]
39. Aerioxide, Aerodisp and Aeroperl. Titanium Dioxide as Photocatalyst. Technical Information. Available online: <https://www.aerosil.com/sites/lists/RE/DocumentsSI/TI-1243-Titanium-Dioxide-as-Photocatalyst-EN.pdf> (accessed on 16 October 2018).
40. Tjeng, L.H.; Meinders, M.B.J.; van Elp, J.; Ghijsen, J.; Sawatzky, G.A.; Johnson, R.L. Electronic Structure of Ag_2O . *Phys. Rev. B* **1990**, *41*, 3190–3199. [CrossRef]
41. Reinoso, J.J.; Leret, P.; Álvarez-Docio, C.M.; Del Campo, A.; Fernández, J.F. Enhancement of UV Absorption Behavior in ZnO-TiO_2 Composites. *Bol. Soc. Esp. Ceram. Vidr.* **2016**, *55*, 55–62. [CrossRef]
42. Jiang, Z.; Huang, S.; Quian, B. Semiconductor Properties of Ag_2O Film Formed on the Silver Electrode in 1 M NaOH Solution. *Electrochim. Acta* **1994**, *39*, 2465–2470. [CrossRef]
43. Vvedenskii, A.; Grushevskaya, S.; Kudryashov, D.; Ganzha, S. The Influence of the Conditions of the Anodic Formation and the Thickness of Ag(I) Oxide Nanofilm on its Semiconductor Properties. *J. Solid State Electrochem.* **2010**, *14*, 1401–1413. [CrossRef]
44. Mills, A.; Wang, J. Photobleaching of Methylene Blue Sensitised by TiO_2 : An Ambiguous System? *J. Photochem. Photobiol. A Chem.* **1999**, *127*, 123–134. [CrossRef]
45. Herrmann, J.-M. Fundamentals and Misconceptions in Photocatalysis. *J. Photochem. Photobiol. A Chem.* **2010**, *216*, 85–93. [CrossRef]
46. Herrmann, J.-M. Photocatalysis Fundamentals Revisited to Avoid Several Misconceptions. *Appl. Catal. B Environ.* **2010**, *99*, 461–468. [CrossRef]

47. Bratsch, S.G. Standard Electrode Potentials and Temperature Coefficients in Water at 298.15 K. *J. Phys. Chem. Ref. Data* **1989**, *18*, 1–21. [[CrossRef](#)]
48. Arimi, A.; Megatiff, L.; Granone, L.I.; Dillert, R.; Bahnemann, D.W. Visible-Light Photocatalytic Activity of Zinc Ferrites. *J. Photochem. Photobiol. A Chem.* **2018**, *366*, 118–126. [[CrossRef](#)]
49. Xu, Y.; Schoonen, M.A.A. The Absolute Energy Positions of Conduction and Valence Bands of Selected Semiconducting Minerals. *Am. Mineral.* **2000**, *85*, 543–556. [[CrossRef](#)]
50. Harifi, T.; Montazer, M.; Dillert, R.; Bahnemann, D.W. $\text{TiO}_2/\text{Fe}_3\text{O}_4/\text{Ag}$ Nanophotocatalysts in Solar Fuel Production: New Approach to Using a Flexible Lightweight Sustainable Textile Fabric. *J. Clean. Prod.* **2018**, *196*, 688–697. [[CrossRef](#)]
51. Hamid, S.; Dillert, R.; Bahnemann, D.W. Photocatalytic Reforming of Aqueous Acetic Acid into Molecular Hydrogen and Hydrocarbons over Co-catalyst-Loaded TiO_2 : Shifting the Product Distribution. *J. Phys. Chem. C* **2018**, *122*, 12792–12809. [[CrossRef](#)]



© 2018 by the authors. Licensee MDPI, Basel, Switzerland. This article is an open access article distributed under the terms and conditions of the Creative Commons Attribution (CC BY) license (<http://creativecommons.org/licenses/by/4.0/>).